Robust Wax Deposition Modeling Incorporating Non-Newtonian Characteristics

Luqman Hakim Ahmad Mahir, Khalid Mateen, Marine Dupoiron, Myriam Darbouret, Thierry Palermo

Robust Wax Deposition Modeling Incorporating Non-Newtonian Characteristics

Luqman Hakim Ahmad Mahir[1], Khalid Mateen[1], Marine Dupoiron[2], Myriam Darbouret[2], Thierry Palermo[3*]

[1]TotalEnergies E&P, 1201 Louisiana St. Suite 1800, Houston, Texas 77002, United States

[2]IFP Energies Nouvelles, Rond-point de l'échangeur de Solaize, 69360 Solaize, France

[3]TotalEnergies E&P, Avenue Larribau, 64018 Pau Cedex, France

* Corresponding Author

Abstract

Wax deposition in sub-sea flowlines during oil production is a well-known problem attributed to the formation of wax crystal induced by ambient cooling. Due to the non-Newtonian characteristics of waxy oil below its wax appearance temperature, the deposit growth can be modeled as a gelation process resulting from the accumulation of wax crystal in the boundary layer which increases the dynamic yield stress leading to the arrest of flow near the wall or gel-fluid interface. In the present study, two modeling approaches were used to match the single-phase turbulent flow wax deposition tests carried out in a 2” flow loop at various conditions. The deposit thickness and wax content evolution with time obtained in the flow loop tests were matched with the models’ simulations. Compared to conventional diffusion approach, which assumes a constant wax content in the depositing layer, the non-Newtonian approach can capture the time varied experimental deposit thickness and wax content both at early and late times. It was also found that assuming fast precipitation kinetics, a typical assumption imposed in these models was found to yield good agreement with the data in all of the tests when employing the non-Newtonian approach.

Keywords: wax deposition, modeling, heat and mass transport, non-Newtonian fluid, yield stress

Introduction

Paraffin or wax fouling is a well-acquainted problem during crude oil production arising from paraffin crystallization triggered by temperature drop during sub-sea oil transport. In cases where wax deposition is inevitable, an estimate of the rate of deposition which relies on mathematical modeling of the deposition physics is invaluable in planning optimal remediation practices.

Numerous mechanisms governing the deposition process have been suggested in the past such as molecular diffusion, thermal driven deposition, shear dispersion, Brownian diffusion, shear stripping, and gravitational settling. For deposition under flow, only molecular diffusion and thermal driven deposition are regarded as primary mechanisms observed at the lab scale.

Thermal drive deposition is a scenario where the deposit growth rate is governed primarily by the rate of heat transfer. Mehrotra et al. considers the process as a moving boundary problem involving the liquid-solid phase transformation[1–4]. Mahir et al. describes the process as the gelation of oil due to the ability of the local fluid to resist flow due to the presence of wax crystals which confers it a yield stress[5,6]. Under the so-called heat transfer-controlled growth, the deposit contains the same composition as the oil due to the process being akin to freezing.

Molecular diffusion has long been regarded as the primary contributor to the formation and growth of wax deposit in the field. Earlier approaches were developed by various

authors such as Burger et al., Rygg, Rydahl and Ronningsen et al. and Singh et al. which employ a 1-D mass balance utilizing the Fickian diffusion equation[7,8]. In this approach, the deposition rate, in terms of the growth of the thickness, is governed by the diffusive flux as well as the concentration of wax crystal assumed in the depositing layer. Typically, this wax crystal concentration is set to be a constant or tuned to match experimental data.

The Classical Approach to Modeling Molecular Diffusion Growth

Molecular diffusion of wax molecules arises from the creation of a concentration gradient triggered by the change in wax solubility from the bulk to the wall due to temperature differences. Since the first work by Burger et al., the deposit growth rate has been more or less based on the diffusive flux of soluble wax at the wall or moving gel-fluid interface[9]:

$$\rho\phi_i\frac{d\delta}{dt} = J_{to\ interface} = D_{wo}\frac{\partial C}{\partial r}\bigg|_i \tag{1}$$

where ϕ_i is the solid wax fraction in the depositing layer. Later work by Singh et al. incorporated a term to account for the diffusion in the gel due its porosity which allows internal diffusion to take place leading to the phenomenon referred to as deposit aging[7,10]. Figure 1 is a cartoon depicting the simultaneous occurrence of this so-called external and internal diffusion.

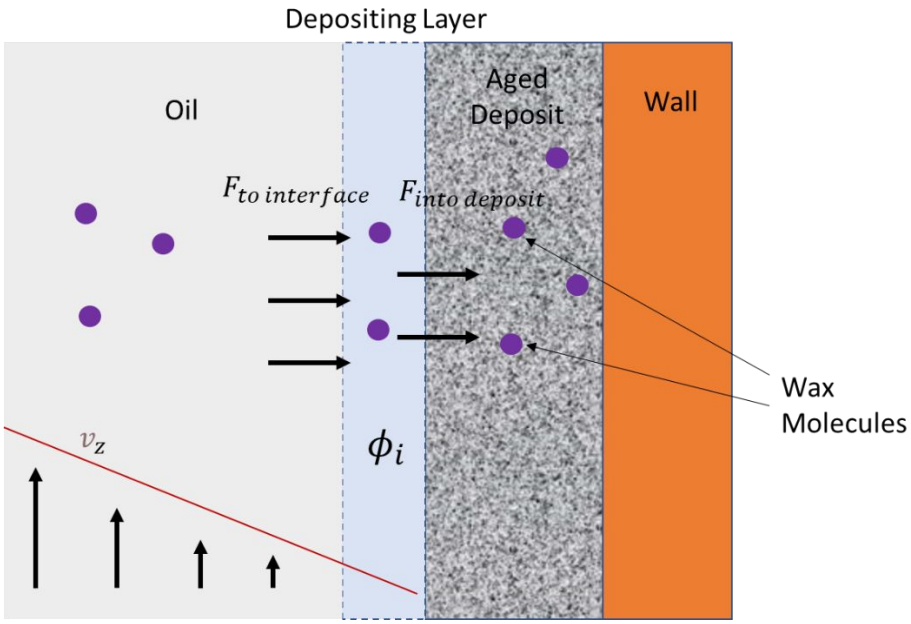

Figure 1: The net diffusion of wax molecules results in the accumulation of solid wax and deposit growth.

The solid wax concentration in the depositing layer increases with time due to the diffusion towards the deposit-oil interface is higher in magnitude than the diffusion into the deposit due to decreasing diffusivity and decreasing concentration driving force going from the bulk to the wall. The deposit growth rate in this scenario can be modelled by Equation (2).

$$\rho\phi_i\frac{d\delta}{dt} = J_{to\ interface} - J_{into\ deposit} = D_{wo}\frac{\partial C}{\partial r}\bigg|_{i^+} - D_{eff}\frac{\partial C}{\partial r}\bigg|_{i^-} \quad (2)$$

where D_{eff} is the wax diffusivity in the porous wax deposit which is usually modelled using a combination of the Hayduk-Minhas correlation and Cussler equation[11,12]. ϕ_i in Equations (1) and (2) is usually taken to be a constant that is chosen arbitrarily or tuned to experimental observation. In the model by Singh, either the average total wax content in the current deposit (for thin deposits)[7] or the total wax content in the layer just behind the gel-liquid interface (for thick deposits)[10] is used instead.

Accounting for non-Newtonian Characteristics in Molecular Diffusion Growth

An approach was developed by Benallal et al. and later further improved upon by Zheng et al. to consider the non-Newtonian characteristic of wax oil in single-phase flow deposition calculation[13–15]. The idea is that waxy oil exhibits yield stress when wax crystals are present, which could arrest flow when the flow shear stress is unable to overcome the yield stress. Local yield stress gradually increases over time with the increase in the wax crystal concentration resulted from waxes that diffuse, precipitate, and accumulate locally. Eventually, the local yield stress grows to a point where the shear stress imposed by the flow becomes unable to overcome it, leading to the formation of a gel. Benallal et al. employ the Bingham plastic constitutive equation in a laminar flow case while Zheng et al. use the Herschel-Bulkley constitutive equation in both laminar and turbulent flow cases.

Under flow conditions where the initial local yield stress near the wall is already much higher than the shear stress imposed by the flow, the deposit growth is expected to be thermal driven as has been seen in some studies. On the other hand, the deposit growth rate would be mass transfer driven when the concentration of solid required for gelation to take place is much higher than the concentration in the existing oil, such as in situations where the oil has low solid wax content or the flow shear stress is relatively high, both of which are typical in field cases[5,6].

In terms of mathematical modeling, the solid wax crystal content in the depositing layer ϕ_i in Equation (5) is no longer ambiguous but is governed by the momentum balance involving the yielding behavior of the waxy oil layer. Zheng and co-workers described the mathematical implementation in full detail[14,15].

The objective of this work was to assess and compare the predictive performances of the non-Newtonian approach and the conventional diffusion approach to modeling wax deposition. The lack of rheological characterization in published data on wax deposition made it impossible to reasonably apply the non-Newtonian model to run simulations of previously published deposition data. Consequently, a thorough flow loop experiments that were accompanied by a thorough rheological characterization of the fluid used was conducted in this work where the results can be compared in a fair manner to the model simulation.

Experimental Section

Materials

A viscous crude oil with a wax appearance temperature of 26.6°C was used in this study. Figure 2 shows the oil precipitation curve measured through differential scanning calorimetry.

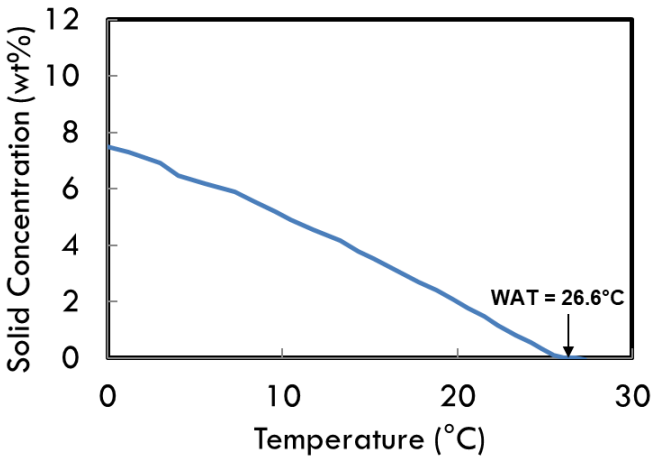

Figure 2: Wax precipitation curve for the crude oil used in this study.

Non-Newtonian Characterization

To obtain yield stress as a function of solid wax fraction, rheological characterization experiments were conducted using a DHR3 (TA Instruments) controlled-stress rotational rheometer. Crude oil samples were first heated up to 60°C then subjected to a temperature ramp down during which they were cooled under a constant shear rate down to a final temperature of 0°C. The cooling rate was kept at -1°C/min. Figure 3 shows the apparent viscosity obtained from this protocol at constant shear rates of 100, 200, 500 and 600 s^{-1}.

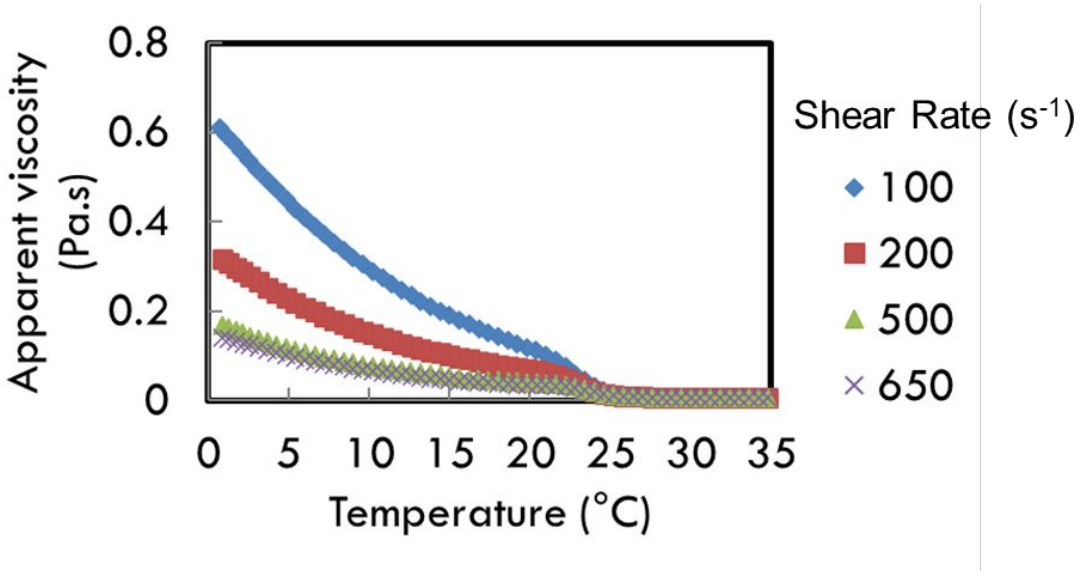

Figure 3: Apparent viscosity of the crude oil used in this study as a function temperature when subjected to cooling at -1°C/min under various constant shear rates.

To utilize the data from Figure 3 in the non-Newtonian wax deposition model, flow curves (shear stress vs. shear rate) at different temperatures were generated and fitted using the Herschel-Bulkley constitutive law. Figure 4 summarizes the scheme used to obtain the Herschel-Bulkley parameters for the simulations. From the Herschel-Bulkley fit of each flow curve, the flow index n, flow consistency K and the yield stress τ_y were obtained as a function of temperature. It should be noted that for these data flow index n was found close to 1, thus reducing the non-Newtonian law to simply a Bingham Plastic. Using the precipitation curve generated from DSC, the relationship between solid wax weight fraction and K and τ_y were established (polynomial or exponential function) and used in the simulations.

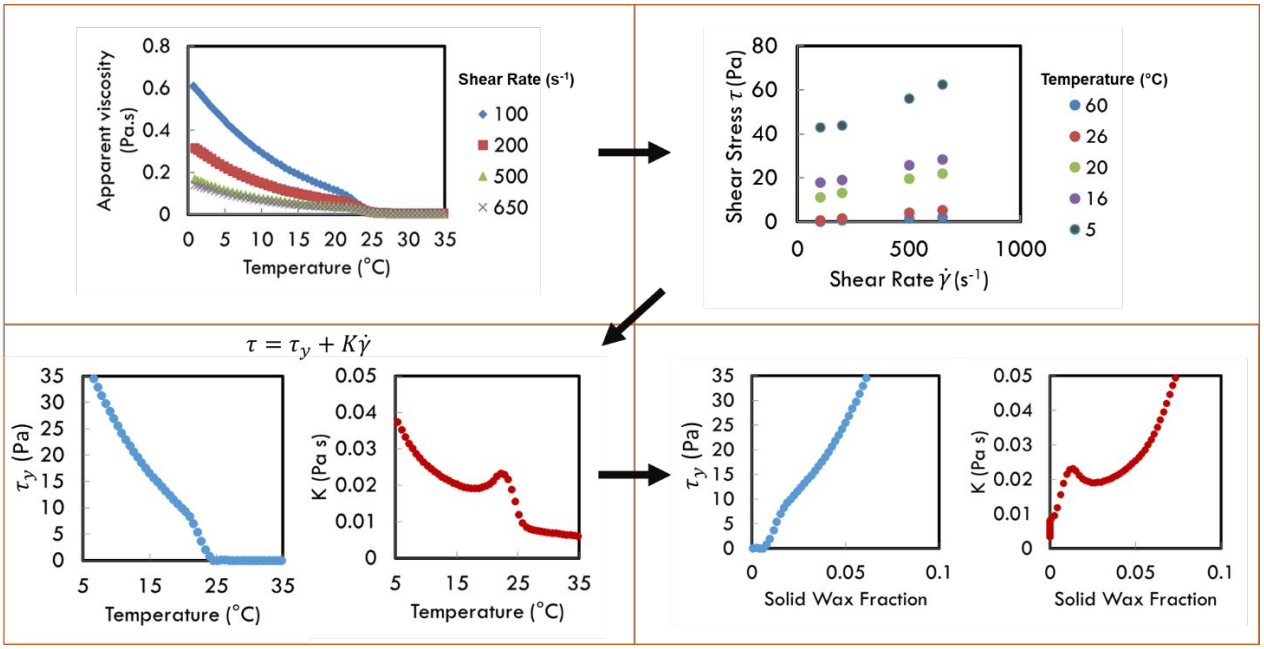

Figure 4: Summary of the methodology used to obtain the non-Newtonian (Herschel-Bulkley/Bingham Plastic) parameters from the measured apparent viscosity data.

Flow Loop Experiments

A set of flow loop experiments at various inlet oil temperature and flow rate conditions were carried out at an IFP Energies Nouvelles (IFPEN) flow loop facility in Solaize, France. All experiments were performed under turbulent single-phase flow conditions. Wax deposit thickness was measured indirectly through an energy balance calculation based on the evolution of the temperature drop with time across the test section resulting from the deposit formation. This approach captures the time-dependent evolution of the deposit thickness. To back calculate the deposit thickness that would result in the temperature drop measured from the experiment, equation (3) was used:

$$h_0 = \frac{1}{\frac{d_1}{(d_1 - 2\delta)h_1} + \frac{d_1}{2\lambda_d}\ln\left(\frac{d_1}{d_1 - 2\delta}\right) + \frac{d_1}{d_2 h_{ext}}} \qquad (3)$$

where h_0 is the overall heat transfer coefficient, d_1 is the pipe internal diameter, d_2 is the pipe external diameter, δ is the deposit thickness, λ_d is the deposit thermal conductivity, h_1 is the internal flow heat transfer coefficient and h_{ext} is the cooling water heat transfer coefficient. λ_d and h_{ext} were taken to be 0.2 W/m/°C and 1800 W/m^2/°C respectively, while the value of h_1 for each test was estimated based on the temperature profile obtained from the deposition simulation. In equation (3), h_0 was obtained using equation (4):

$$h_0 = \frac{m_{crude} C_{p,crude} \left(T_{crude}^{in} - T_{crude}^{out}\right)}{\pi d_1 L \Delta T_{LM}} \tag{4}$$

where m_{crude} is the oil mass flow rate, $C_{p,crude}$ is the oil specific heat capacity, T_{crude}^{in} is the oil inlet temperature, T_{crude}^{out} is the oil outlet temperature, L is the test section length and T_{LM} is the log mean temperature difference calculated using Equation (5):

$$\Delta T_{LM} = \frac{\left(T_{crude}^{in} - T_{gly}^{out}\right) - \left(T_{crude}^{out} - T_{gly}^{in}\right)}{\ln\left(\frac{T_{crude}^{in} - T_{gly}^{out}}{T_{crude}^{out} - T_{gly}^{in}}\right)} \tag{5}$$

where T_{gly}^{in} and T_{gly}^{out} are the glycol water inlet and outlet temperatures respectively.

Five experiments were carried out with their conditions summarized in Table 1.

Table 1: Experimental conditions of the flow loop tests.

Test	$T_{oil,inlet}$ (°C)	$T_{coolant,inlet}$ (°C)	T_{wall} (°C)	Flow rate (m^3/h)	Estimated Wall Shear Stress (Pa)	Duration (h)
D1	27.5	8	9.5	7.5	3.5	40

G1	27.5	17	20.2	7.5	3.5	40
C1	23.5	20	21	15	12	150
B1	27.5	21.2	23.1	15	12	50,150
E1	27.5	23.5	25.6	15	12	150

At the end of each experiment, a sample of the deposit was collected for deposit composition analysis. Calorimetric analyses on the samples were performed using a Mettler Toledo DSC 1. Two methods were employed to obtain the precipitation curve and wax content from the thermograms: either the ratio between enthalpy areas or the use of a theoretical enthalpy value of ΔH= 200 J/g. Both methods lead to converging results.

Model & Simulation Parameters

The dimensions and other relevant physical characteristics of the flow loop characteristics were provided by IFP Energies Nouvelles and are summarized in Table 2. Fluid and wax density, thermal conductivity, heat capacity and kinetic parameter assumed are shown in Table 3.

Table 2: Flow loop dimensions and physical properties.

Pipe length L	5.9 m (D1) 6.9 m (G1, E1 & B1)
Pipe inner diameter D_i	0.0525 m
Pipe outer diameter D_o	0.08 m

Wall thermal conductivity k_{wall}	14 W/m/°C
Heat transfer coefficient between outer pipe and cooling fluid h_{ext}	600 – 1500 W/m^2/°C

Table 3: Oil and wax properties.

Fluid & wax density ρ	841 kg/m^3
Fluid and wax thermal conductivity k	0.2 W/m/°C
Fluid and wax specific heat capacity $\hat{c}_p$	2100 J/kg/°C
Precipitation rate constant k_r	10^3
Crystal aspect ratio K_α (used to calculate the D_{eff} using the Cussler equation)	5

Yield stress as a function of the solid fraction shown in Figure 3 was fitted to a piecewise defined function to be applied in the yield stress-based model.

Irrespective of which deposition model is considered, the same heat and mass transport equations are involved. Assuming paraffins can be lumped together as a single species existing as a soluble wax or precipitated wax, one can arrive at the respective mass balances shown in Equations (6) and (7) for flow in a cylindrical pipe assuming axisymmetry.

$$\frac{\partial C_s}{\partial t} + v_z\frac{\partial C_s}{\partial r} = \frac{1}{r}\frac{\partial}{\partial r}\left[(D_{eff} + \epsilon_i)\frac{\partial C_s}{\partial r}\right] - k_r(C_s - C_{s,eq}) \quad (6)$$

$$\frac{\partial C_p}{\partial t} + v_z \frac{\partial C_p}{\partial r} = \frac{1}{r}\frac{\partial}{\partial r}\left[(\epsilon_i)\frac{\partial C_p}{\partial r}\right] + k_r(C_s - C_{s,eq}) \quad (7)$$

The energy balance can be derived in a similar manner as follows:

$$\hat{\rho c_p}\frac{\partial T}{\partial t} + \hat{\rho c_p} v_z \frac{\partial C_p}{\partial r} = \frac{1}{r}\frac{\partial}{\partial r}\left[(\alpha + \epsilon_H)\frac{\partial T}{\partial r}\right] + \Delta H_{crys}\frac{\partial C_p}{\partial t} \quad (8)$$

For the centerline boundary condition, symmetry is assumed at r = 0 in all three equations. At the wall, zero mass flux is assumed in equations (7) and (8) while in equation (9) a constant wall temperature was used based on the average wall temperature measured in the experiment.

In both approaches, the soluble wax diffusivity is calculated using the Hayduk and Minhas correlation to obtain the solid-free diffusivity which is then used to obtain the effective diffusivity based on the Cussler model[11,12]. The crystal aspect ratio parameter K_α for the internal diffusion is taken to be 5 in all simulations. Additionally, precipitation rate is assumed to be very fast by taking k_r to be 10^3 s^{-1}.

In the yield-stress approach, Equations (6), (7), and (8) are solve simultaneously with the hydrodynamic calculations outlined in Zheng et al. 2017 to obtain axial and radial profiles of temperature, wax concentration, as well as the axial profile of deposit thickness, all as a function of time. In the conventional diffusion approach, Equation (2) in which ϕ_s must be specified is used in place of Zheng's hydrodynamic calculations to calculate the change in deposit thickness at each axial node. To probe the sensitivity of the deposition behavior on ϕ_s, simulations at several ϕ_s values were carried out.

The average deposit thickness along the axis and the average total wax concentration in the deposit from the simulations were compared with the experiments.

Results and Discussions

Experimental Deposit Thickness Results

The experimental time varying deposit thickness obtained from solving Equations 3 through 5 are shown in Figure 4. Upon examining the early times growth, it was observed that the tests D1 and G1 had a very rapid growth taking place during the first 30 minutes (whose thicknesses grew to 0.9mm and 0.2mm respectively) followed by a more gradual growth rate for the rest of the duration of the experiment, whereas growth rates in tests C1, B1 and E1 were gradual from the beginning. To help with interpreting these results, a mapping of the different experiments as a function of their flow shear stress and wall temperature in relation to the oil yield stress is plotted in Figure 5. This diagram guides the expectations for how the deposit formation under the different conditions would take place. If the experiment falls below the measured yield stress curve, the deposit growth is expected to be rapid initially due to oil gelation followed by a more gradual growth governed by molecular diffusion. On the other hand, if the experiment lies above this yield stress are expected to behave in the classical molecular diffusion mechanism from the very beginning. Based on Figure 5, tests D1 and G1 are expected to be subjected to oil gelation at the onset of deposition while C1, B1 and E1 are not. Indeed, the results in Figure 4 confirm these expectations. From here on, tests D1 and G1 will be grouped together as tests that are below the gelation envelope, while tests C1, B1 and E1 will be identified as tests that are above the gelation envelope.

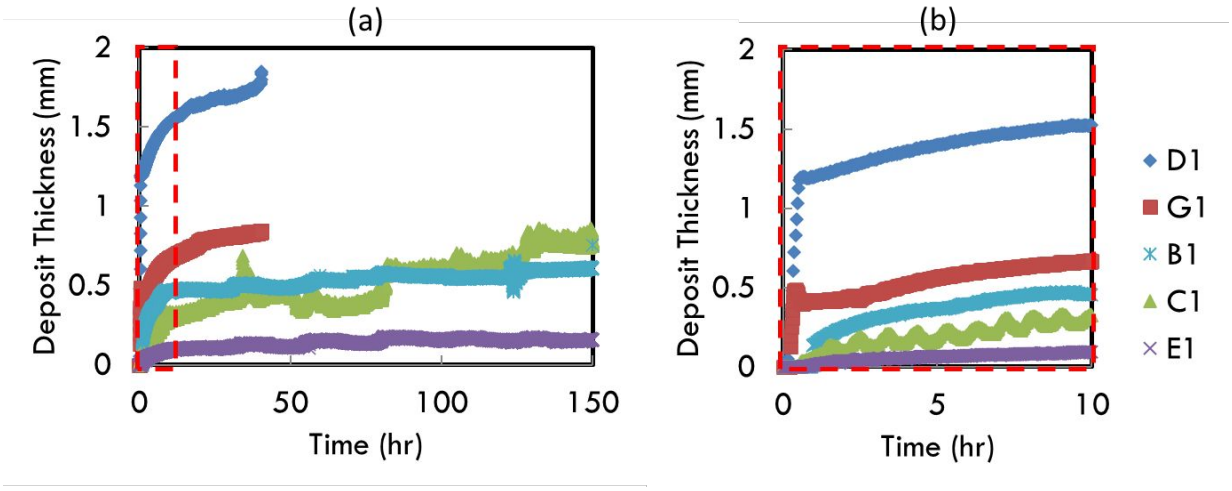

Figure 5: Experimental deposit thickness for (a) the entire duration and (b) the first 10h obtained from solving Equations 3, 4 and 5 based on temperature probe measurements.

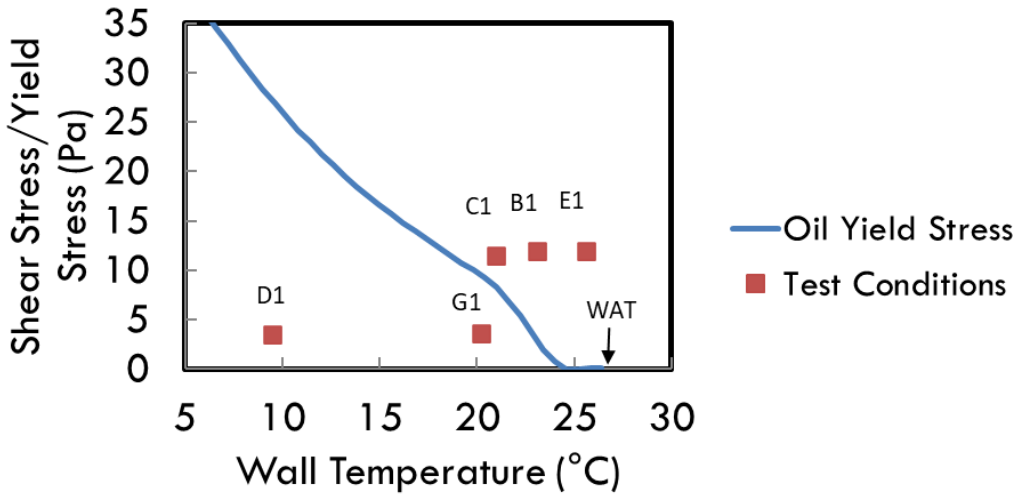

Figure 6: Calculated shear stress and wall temperature of the flow loop tests in relation to the measured oil yield stress.

Table 4 presents the deposit total wax content measured from the experiments.

Table 4: Deposit total wax content results from DSC.

Test	$T_{oil,inlet}$ (°C)	T_{wall} (°C)	Duration (hr)	Deposit total wax content (wt%)
D1	27.5	9.5	40	30
G1	27.5	20.2	40	40
C1	23.5	21	150	60

B1	27.5	23.1	50	45
			150	60
E1	27.5	25.6	150	60

Comparison between Flow Loop Experiment and Simulation Results

Wall Temperature Below Gelation Envelope

Test D1 was performed with an inlet oil temperature of 27.5°C (1°C above the WAT) and wall temperature of 8°C with a constant flow rate of 7.5 m^3/h. As previously pointed out based on the yield stress-shear stress map in Figure 6, this experiment was expected to yield a rapid initial growth due to oil gelation, followed by a slower growth by molecular diffusion. The experimental thickness result confirms this behavior.

Figure 7 shows the prediction of deposit thickness using the two modeling approaches as compared to the experimentally measured thickness. The conventional approach is incapable of capturing the rapid initial growth rate, in contrast to the non-Newtonian approach which accurately captures the deposit growing to 1mm during the first 30 minutes. It should be reminded that thermodynamic equilibrium was assumed in all these simulations for comparison between the models.

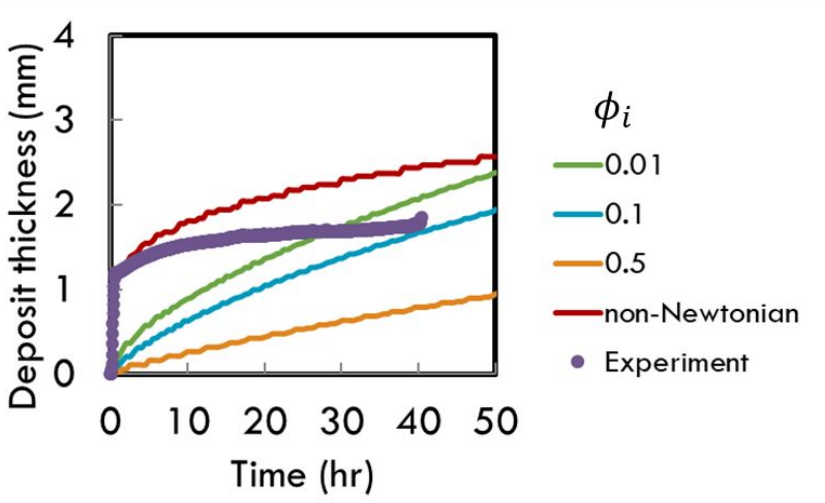

Figure 7: Predicted deposit thickness using the two models as compared to the experimentally measured thickness from test D1.

It is also interesting that under these conditions and unlike the tests above the gelation envelope, the deposit growth rate predicted by the conventional model is more strongly dependent on ϕ_i likely due to the lower wall temperature which allows for a thicker deposit formation.

Figure 8 shows the deposit wax content evolution with time predicted by the two models compared to the experimental data. With the exception of the conventional model with $\phi_i = 0.5$, both the conventional model and the non-Newtonian predict comparable deposit wax content at 40hr due to the same transport approaches used. Their time trajectory behaviors however are not similar due to their different thickness time trajectory. This good matching in terms of deposit composition between both models and the experiment implies that the aging and diffusion rate were reasonably modeled.

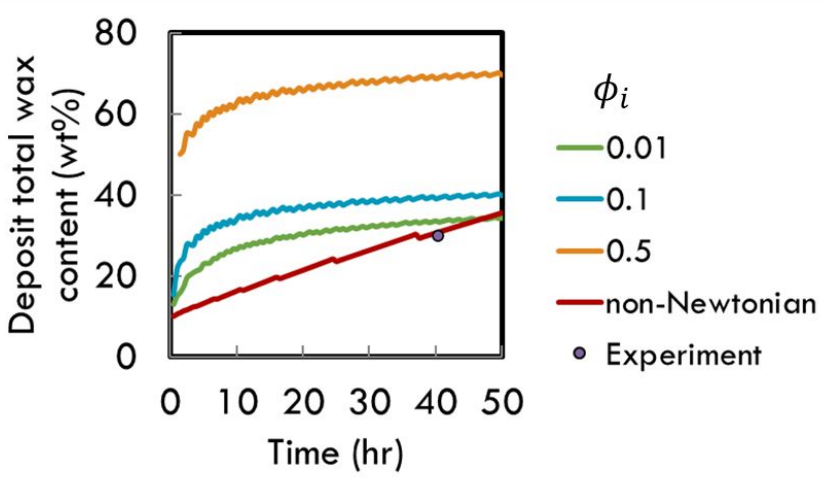

Figure 8: Predicted deposit total wax content using the two models as compared to the experimentally measured value from test D1.

The comparison between predicted and the measured deposit thickness and deposit compositions for test G1 are shown in Figures 9 and 10 respectively. Similar to test D1, the non-Newtonian model is capable of capturing both the initial fast growth due to gelation and the more limited growth at longer times to due to higher shear stress at the interface resulted from the deposit formation. Assuming ϕ_s between 0.01 and 0.1 in the conventional model underpredicts the deposit thickness although it yielded a reasonable wax content of the aged deposit. A higher ϕ_s would perform worst as seen with ϕ_s of 0.5. The extent of gelation is less significant in test G1 due to its higher wall temperature.

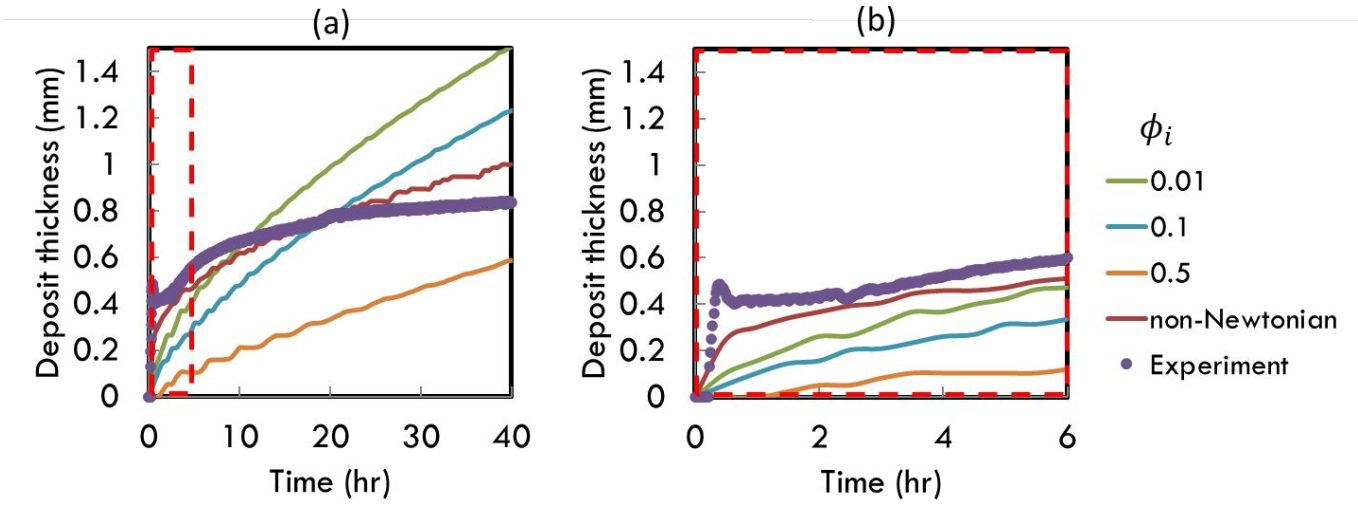

Figure 9: Experimental and predicted deposit thickness for (a) the entire duration and (b) the first 6h of test G1.

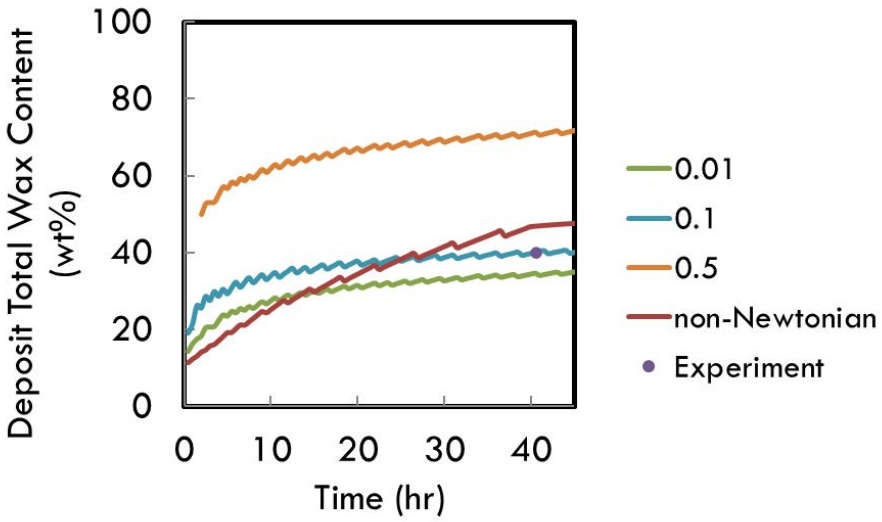

Figure 10: Experimental and predicted deposit wax content from test G1.

Wall Temperature Above the Gelation Envelope

Test E1 was performed at a flow rate of 15m^3/h with a wall temperature of approximately 25.6°C. The time dependent deposit thicknesses simulated using the conventional diffusion model and the non-Newtonian model are plotted against the experimentally measured thickness in Figure 11. As seen in Figure 11, while a higher ϕ_s results in a slower growth rate as expected due to the formation of a more solid

depositing layer, the change in ϕ_s has to be large in order to observe a notable decrease in the deposit growth rate, at least initially. Furthermore, time trajectory deposit thicknesses predicted by the conventional model are not far off from that predicted by the non-Newtonian model. To explain these observations, Equation 2 must be pondered upon. Test E1 has the lowest driving force for diffusion due to the small temperature gradient, thus the limiting factor for the growth rate is the rate by which soluble waxes get transported to the wall or gel-oil interface.

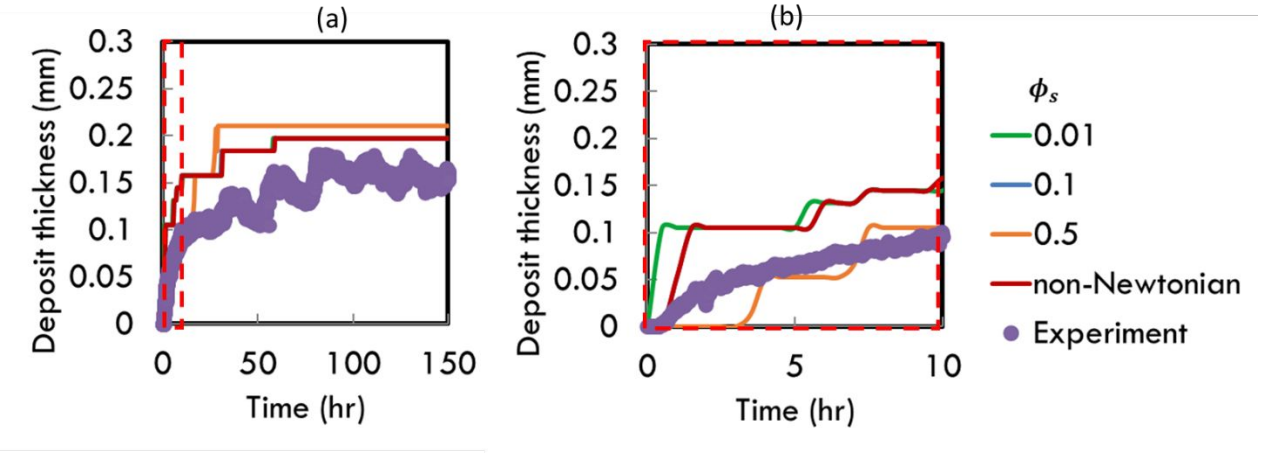

Figure 11: Predicted deposit thickness using the non-Newtonian approach and the conventional mass transfer approach at various ϕ_s for test E1.

To assess the performance of the mass transfer modeling of both models, the predicted deposit total wax content was compared with experimental data at t = 150h as shown in Figure 12 respectively. The predictions between the different simulations are comparable to one another consistent with the thickness results in Figure 11.

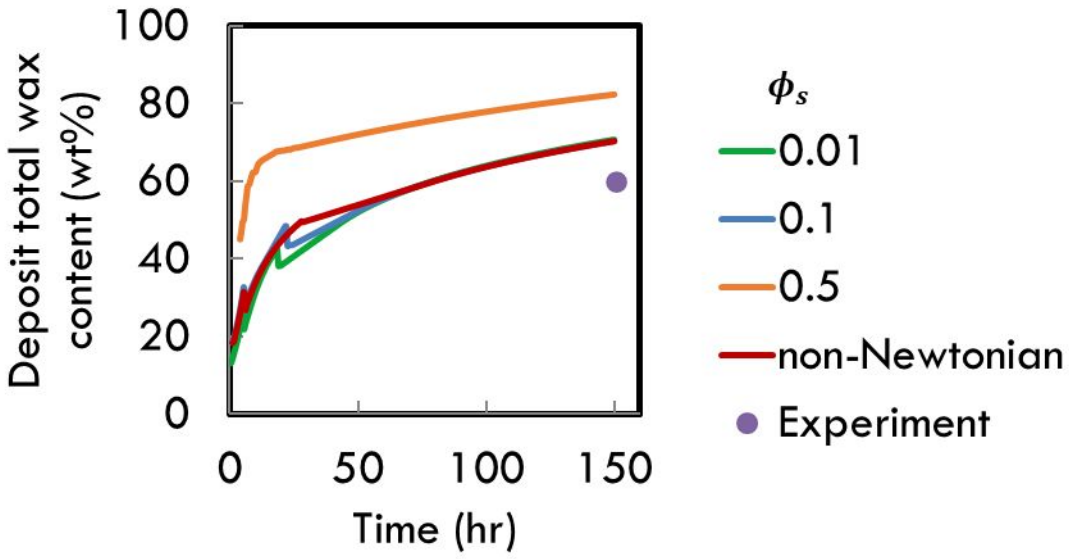

Figure 12: Predicted deposit total wax content using the non-Newtonian approach and the conventional mass transfer approach at various ϕ_s for test E1.

Test B1 was performed at the same flow rate as E1 at 15m^3/h but with a lower wall temperature of approximately 23.1°C yielding a thicker deposit. The time dependent deposit thicknesses simulated using the conventional diffusion model and the non-Newtonian model are plotted against the experimentally measured data in Figures 13 and 14. Unlike test E1, there is a more notable decrease in the deposit growth rate during the first 30h with increasing ϕ_s. As a result, characterizing ϕ_s is more important in this scenario. As shown in Figure 13, ϕ_s = 0.03 gives the closest prediction to the experiment, which also overlaps with the non-Newtonian model prediction. This observation is consistent with the non-Newtonian characteristics of the fluid

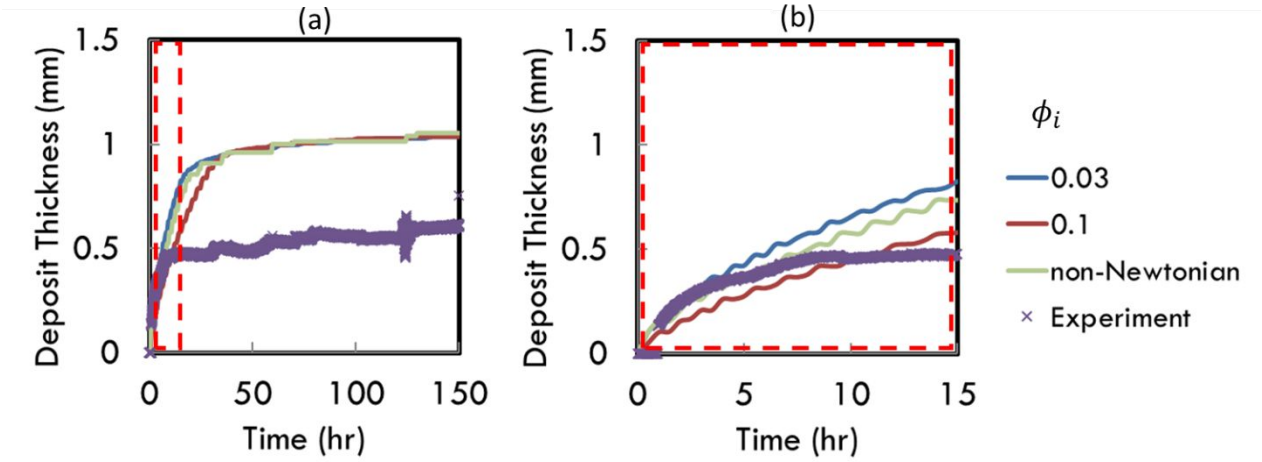

Figure 13: Predicted deposit thickness using the non-Newtonian approach and the conventional mass transfer approach at various ϕ_s for test B1.

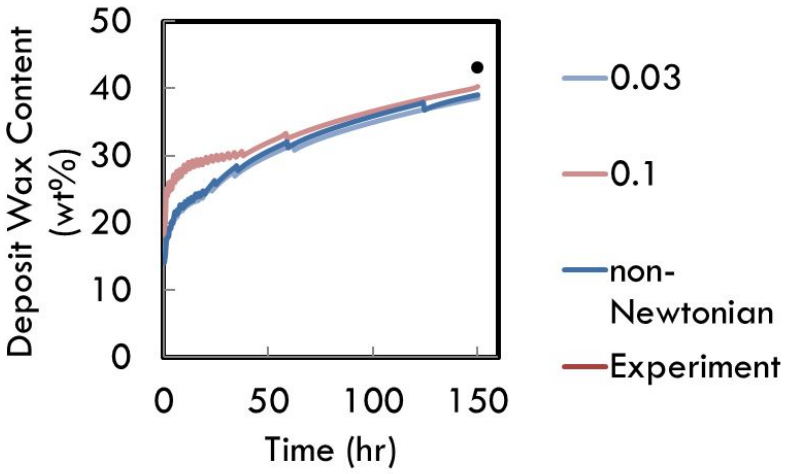

Figure 14: Predicted deposit total wax content using the non-Newtonian approach and the conventional mass transfer approach at various ϕ_s for test B1.

The closeness in the predictions between the conventional and non-Newtonian models for these cases implies that under flow and temperature conditions where the deposition rate is slow and limited by the rate of diffusion of wax to the wall or interface, the conventional approach can perform just as well as long as the diffusion and other mass transport characteristics including the deposit aging are captured.

Conclusions

A set of flow loop experiments were carried out at various oil temperature, wall temperature and flow rates. Two modelling approaches were used to match the experimental data: the classical molecular diffusion approach, and the non-Newtonian approach.

From the comparison between the model predictions and the experimental data, it was found that the usage of dynamic yield stress in the non-Newtonian approach performs more satisfactorily compared to the classical approach. Both early time and late time deposition rates are captured by the non-Newtonian model with changing flow rate and temperature driving force using a single value assigned to the precipitation kinetic and aging parameters. This can be attributed to the unambiguous modeling of the necessary solid fraction required to immobilize a flowing oil, which is the basis for the deposition mechanism observed in single phase flow in the flow loop. The predictability of the non-Newtonian approach across different flow and temperature conditions found in this study demonstrated its scalability when used in field cases.

Acknowledgement

The authors would like to thank the EasyWAX JIP participants for allowing access to the experimental data and various technical discussions.

Notation

t	Time (h)
ρ	Density of the oil and deposit (kg/m^3)
ΔH	Specific latent heat of wax crystallization (J/kg)

δ	Deposit thickness (m or mm)
k	Thermal conductivity of oil and deposit (W/m/°C)
$\hat{c}_p$	Specific heat capacity of oil and deposit (J/kg/°C)
α	Thermal diffusivity of oil and deposit (m^2/s)
ϵ_H	Thermal eddy diffusivity (m^2/s)
T	Temperature of the oil or deposit (°C)
$T_{oil,inlet}$	Temperature of oil at the inlet (°C)
$T_{coolant,inlet}$	Temperature of circulating coolant (°C)
T_{wall}	Temperature of pipe wall (°C)
T_i	Temperature at the deposit-oil interface (°C)
r	Radial coordinate (m)
z	Axial coordinate (m)
D_i	Inner diameter of pipe (m)
D_o	Outer diameter of pipe (m)
L_{pipe}	Pipe length (m)
C_s	Soluble (i.e., dispersed) n-C28 concentration (kg/m^3)
$C_{s,eq}$	Soluble wax concentration at the solubility limit (kg/m^3)
C_p	Precipitated wax concentration (kg/m^3)
k_r	Precipitation rate constant (s^{-1})

$D_{w/o}$	Soluble wax diffusivity in precipitate-free oil based on the Hayduk-Minhas equation (m^2/s)
D_{eff}	Effective soluble wax diffusivity (m^2/s)
ϵ_i	Mass eddy diffusivity (m^2/s)
μ	Viscosity of precipitated wax-free oil (mPa s)
V_A	Molar volume of wax molecule (cm^3/mol)
K_α	Dimensionless wax crystal aspect ratio
v_z	Axial velocity of oil (m/s)
τ_y	Local yield stress (Pa)
τ_w	Wall shear stress (Pa)
K	Consistency index (Pa s^n)
n	Flow index
ϕ_s	Solid wax fraction in the depositing layer

References

1. Bhat N V., Mehrotra AK. Modeling of deposit formation from “Waxy” mixtures via moving boundary formulation: Radial heat transfer under static and laminar flow conditions. *Ind Eng Chem Res*. 2005;44(17):6948-6962. doi:10.1021/ie050149p
2. Bidmus H, Mehrotra AK. Measurement of the liquid-deposit interface temperature during solids deposition from wax-solvent mixtures under sheared cooling. *Energy and Fuels*. 2008;22(6):4039-4048. doi:10.1021/ef800542a
3. Arumugam S, Kasumu AS, Mehrotra AK. Modeling of solids deposition from “waxy” mixtures in “hot flow” and “cold flow” regimes in a pipeline operating under turbulent flow. *Energy and Fuels*. Published online 2013. doi:10.1021/ef401315m
4. Kasumu AS, Mehrotra AK. Solids deposition from two-phase wax-solvent-water “waxy” mixtures under turbulent flow. In: *Energy and Fuels*. ; 2013. doi:10.1021/ef301897d
5. Mahir LHA, Vilas Bôas Fávero C, Ketjuntiwa T, Fogler HS, Larson RG. Mechanism of Wax Deposition on Cold Surfaces: Gelation and Deposit Aging.

Energy and Fuels. Published online 2019. doi:10.1021/acs.energyfuels.8b03139

6. Mahir LHA, Lee J, Fogler HS, Larson RG. An Experimentally Validated Heat and Mass Transfer Model for Wax Deposition from Flowing Oil onto a Cold Surface. *AIChE J*. Published online 2020. doi:10.1002/aic.17063

7. Singh P, Venkatesan R, Fogler HS, Nagarajan N. Formation and aging of incipient thin film wax-oil gels. *AIChE J*. 2000;46(5):1059-1074. doi:10.1002/aic.690460517

8. Rygg OB, Rydahl AK, Ronningsen HP. Wax Deposition in Offshore Pipeline Systems. In: *1st North American Conference on Multiphase Technology*. ; 1998.

9. Burger ED, Perkins TK, Striegler JH. Studies of Wax Deposition in the Trans Alaska Pipeline. *JPT, J Pet Technol*. Published online 1981. doi:10.2118/8788-PA

10. Singh P, Venkatesan R, Scott Fogler H, Nagarajan NR. Morphological evolution of thick wax deposits during aging. *AIChE J*. 2001;47(1):6-18. doi:10.1002/aic.690470103

11. Hayduk W, Minhas BS. Correlations for prediction of molecular diffusivities in liquids. *Can J Chem Eng*. 1982;60(2):295-299. doi:10.1002/cjce.5450600213

12. Cussler EL, Hughes SE, Ward WJ, Aris R. Barrier membranes. *J Memb Sci*. 1988;38(2):161-174. doi:10.1016/S0376-7388(00)80877-7

13. Benallal A, Maurel P, Agassant JF, Darbouret M, Avril G, Peuriere E. Wax deposition in pipelines: Flow-loop experiments and investigations on a novel approach. *Proc - SPE Annu Tech Conf Exhib*. 2008;2:875-891. doi:10.2118/115293-ms

14. Zheng S, Saidoun M, Mateen K, Palermo T, Ren Y, Fogler HS. Wax deposition modeling with considerations of non-Newtonian fluid characteristics. In: *Proceedings of the Annual Offshore Technology Conference*. ; 2016.

15. Zheng S, Saidoun M, Palermo T, Mateen K, Fogler HS. Wax Deposition Modeling with Considerations of Non-Newtonian Characteristics: Application on Field-Scale Pipeline. *Energy and Fuels*. Published online 2017. doi:10.1021/acs.energyfuels.7b00504